Figure S1 Leyman et al.

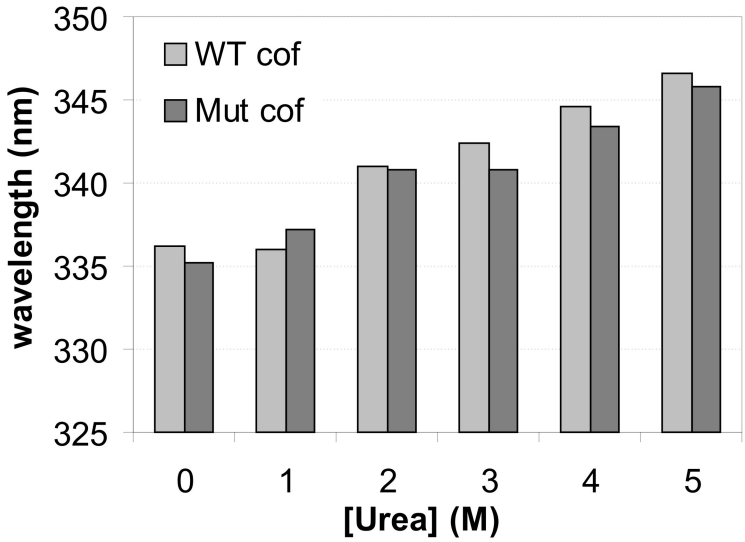

Figure S1. Protein stability of purified WT and D122K cofilin. The shift in maximal wavelength (nm) of the tryptophan emission spectrum (excitation 279 nm) of GST-cofilin, that is induced upon denaturation, is plotted in function of increasing urea concentration. The changes in emission maximum are very similar for WT and D122K cofilin.

Figure S2 Leyman et al.

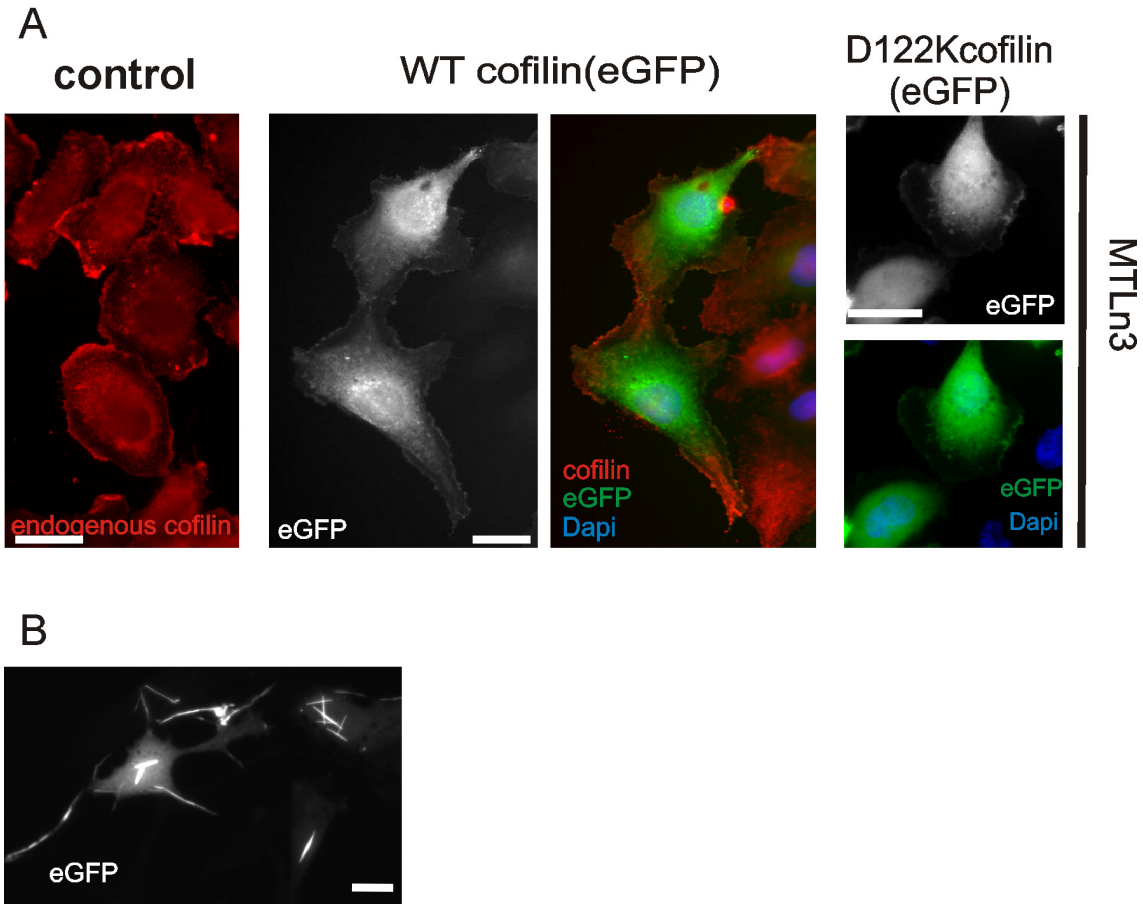

Figure S2. (A) Localization of cofilin (red) and/or the eGFP signal (grey or green) in MTLn3 cells: control cells (left), cells overexpressing eGFP-WT cofilin (middle panels) or eGFP-D122K cofilin (right panels). DAPI (blue) for nuclear staining. Scale bar, 20 µm. (B) Rod formation in cofilin-eGFP overexpressing NIH3T3 cells. Overexpression of both tagged and untagged variants of WT cofilin (as described by others (Jang *et al.*, 2005)) or D122K cofilin induce rod formation in a fraction of a transiently transfected cell population. If present, the cofilin containing rod structures (WT or D122K) localize to the cytoplasm, in the nuclear periphery and in the nucleus of the cells. Selected NIH3T3 cells overexpressing D122K-cofilin-eGFP displaying extensive rod formation are shown. In NIH3T3, the amount of cells with rods is slightly higher upon D122K cofilin-eGFP versus WT cofilin-eGFP overexpression. Rod formation is also apparent using constructs with an amino terminal tag (myc, eGFP) suggesting their occurrence is independent of the tag used, its size or the location at N- or C-terminus of the cofilin protein (data not shown).

Figure S3 Leyman et al.

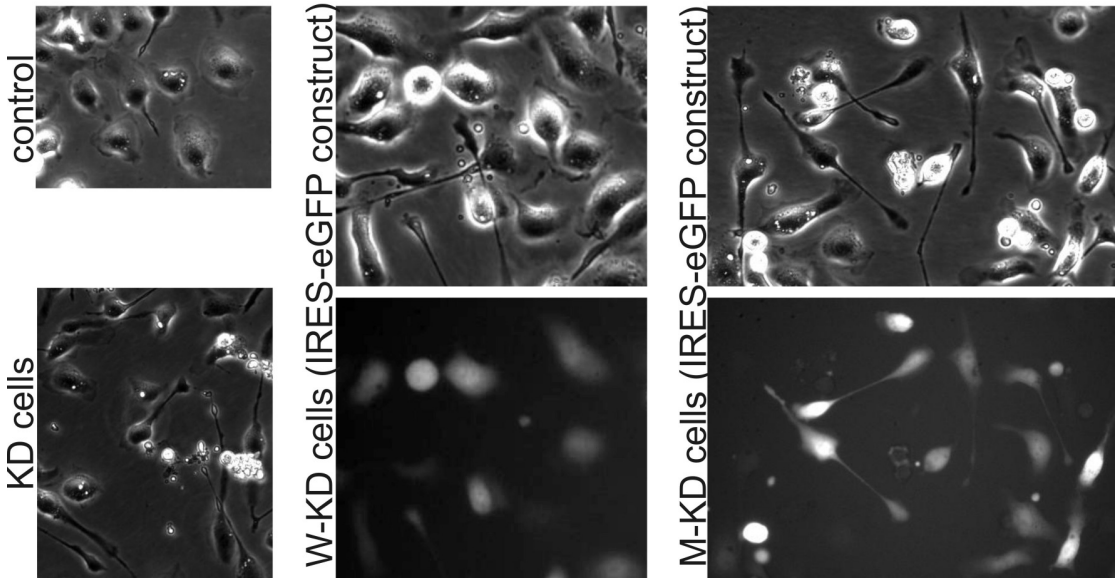

Figure S3. Morphology of KD cells transfected with an Internal Ribosome Entry Site (IRES) construct coding for both untagged cofilin (D122K or WT) and eGFP (as transfection indicator). Phase contrast images and eGFP signals (lower middle and lower right panel) of W-KD (middle) and M-KD (right) cells are shown 18 h after plasmid transfection. Phase contrast images of control and KD cells are shown for comparison (left panels, see also (Sidani *et al.,* 2007)). Exogenous D122K or WT cofilin expressing cells are eGFP-positive. Most fluorescent cells in the W-KD group have reverted to the normal rounded morphology typical for control cells. On the contrary, fluorescent M-KD cells have retained their elongated morphology.

Figure S4 Leyman et al.

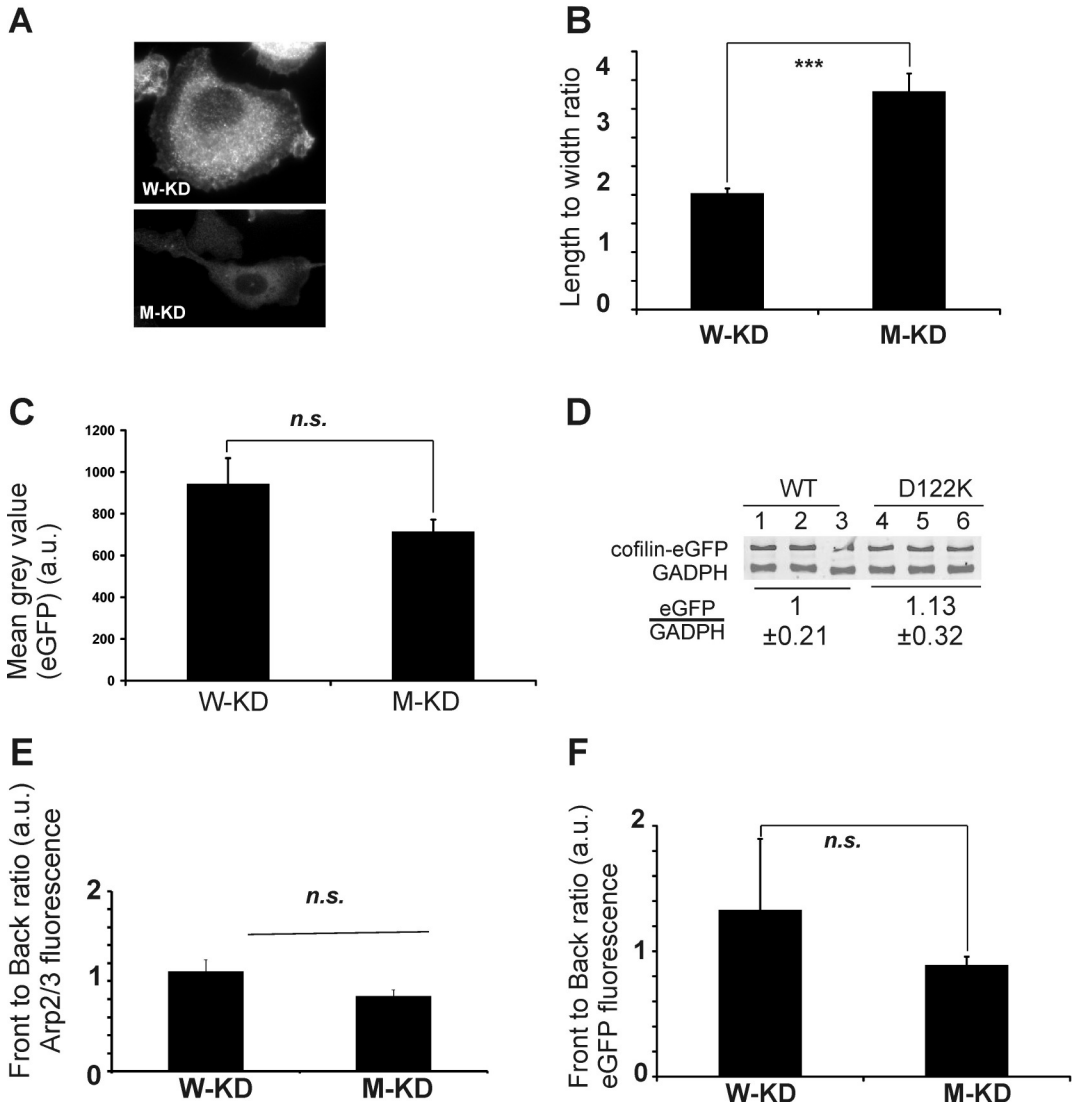

Figure S4. Arp2/3-complex location in cofilin KD cells expressing eGFP-WT (W-KD) or D122K cofilin (M-KD). (A) Immunofluorescence signal for Arp2/3-complex in W-KD and M-KD cells. (B) Mean length to width ratio of the W-KD and M-KD cells (±SEM) confirming the more elongated morphology of the M-KD cells used in this experiment. *** $p<0.001$ (C) Mean grey value corresponding to eGFP intensity in W-KD and M-KD cells. n.s., not significant: $p = 0.11$. This indicates eGFP-WT or D122K cofilin are expressed to comparable levels. (D) Quantification by Western blotting using anti-eGFP antibody of expression levels of eGFP-WT or D122K cofilin in MTLn3 cells from three independent transfection experiments. The signal obtained for GAPDH was used to correct for equal protein loading on the gel. The ratio eGFP vs GAPDH was set to one for the WT condition. (E) Mean front to back ratio of Arp2/3-complex signal in W-KD (n=17) and M-KD cells (n=14); error bars: SEM. Front and back are defined by drawing a line through the geometrical centre of a cell and intensities in the two cell halves are measured. n.s., not significant: $p = 0.075$. (F) Mean front to back ratio of eGFP signal in W-KD and M-KD cells are not significantly different ($p=0.09$); error bars: SEM.

Figure S5. Random migration of different MTLn3 cell populations (time lapse movies). Experimental set up is as in Figure 6. W- and M-KD cells express WT and D122K cofilin as V5-tagged cofilin, as also used in (Sidani *et al.* 2007). **Video 1 – 4:** migration under serum conditions of control, KD, W-KD or M-KD MTLn3 cells, respectively. Cells were recorded during 45 min at 37°C. Images were taken every 30 s and are displayed at 10 frames/second (speed x 600). D122K cofilin overexpression does not rescue the elongated phenotype of KD cells (see Figure 5) and statistical analysis revealed that M-KD cells significantly migrate in a more directional manner than W-KD cells (see Figure 6).

Figure S6. Protrusive activity upon EGF stimulation of the different MTLn3 cell populations (time lapse movies). Experimental set up is as in Figure 8. W- and M-KD cells express WT and D122K cofilin as V5-tagged cofilin, as also used in (Sidani *et al.* 2007). **Video 5 - 8** illustrate the effect of 5 nM EGF-bath stimulation on starved control, KD, W-KD or M-KD MTLn3 cells, respectively. Images were taken every 10s during 10 min at 37°C and are displayed at 100 frames/second (speed x100). Like KD cells, M-KD cells mainly protrude at the pole whereas W-KD cells protrude and form new lamellipodia along their entire cell perimeter. Measurements of the EGF-induced increases along the four cell axes is shown in Figure 7D. M-KD cells protrude more efficiently than KD cells (see Figure 7D and fold increase in overall cell area in 7A).

Supplemental Methods

Analysis of video-microscopy of random cell migration of fibroblasts: image processing and description of derived migration parameters

NIH3T3 cells, plated on fibronectin (5.7 µg/cm^2), were allowed to spread for at least 16 h before start of image acquisition. They were imaged every 5 min for 4 h using a inverted microscope (Olympus IX71) with a 10x NA 0.3 infinity-corrected objective equipped with a monochrome SPOT-RT CCD digital camera (Progress Control). We used the cell-tracking algorithm developed by (Debeir *et al*., 2005) to establish and quantitatively analyze the trajectories of individual cells. For each trajectory, the software computes several parameters that are speed and persistence related (see (Debeir *et al.*, 2005) and Figure 3B (main text)). **Maximum distance from the origin** (**MDO**, in µm) is the distance that maximally occurs between the origin of the cell's trajectory and a subsequent position along the trajectory. **Hull area** (in µm^2) is the area of the convex polygon (i.e. in which every internal angle is less than 180 degrees) that includes all the points of the cell trajectory and is a measure for the area covered by the migrating cell. The **average speed** (in µm/min) over the total time of observation is the average of the migration speed of the cell computed in each time frame of the sequence (i.e. the mean length of the cell trajectory covered per time unit).
We here add an additional parameter, **SLOPE** (in frame^{-1}) that is a persistence feature derived as follows:
For each trajectory interval (of specific step size or number of consecutive frames), we compute the net distance between the start and end position of the interval, $T_{step}(i)$, and its curvilinear distance (along trajectory), $S_{step}(i)$, with $T_{step}(i) < S_{step}(i)$ except for a straight line were $T_{step}(i) = S_{step}(i)$ (see figure).
From this, we compute:

This value is averaged for all possible intervals of the trajectory:

$$R_{step}(i) = \log_{10} \frac{T_{step}(i)}{S_{step}(i)}$$

$$R_{step}^{avg} = \frac{\sum_{i=0}^{i=N-step+1} R_{step}(i)}{N - step + 1}$$

This average expresses the tendency of a trajectory to be close to a straight line with respect to a certain number of time steps. A trajectory for which this average is close to zero for increasing step size indicates that most of the trajectory is straight and thus that the cell is moving highly directional. On the contrary, a fast descending value for this averaged R_{step} indicates that the trajectory displays little persistence in direction.

The SLOPE parameter is the slope of a linear fitting on the first points (arbitrarily set to 10 with respect to our experimental conditions) of the curve obtained by plotting the averaged R_{step} versus step size.
SLOPE is always lower or equal to 0, and is, in absolute values, inversely correlated to persistence of cell migration, i.e. a more negative value represents lower persistence**.**

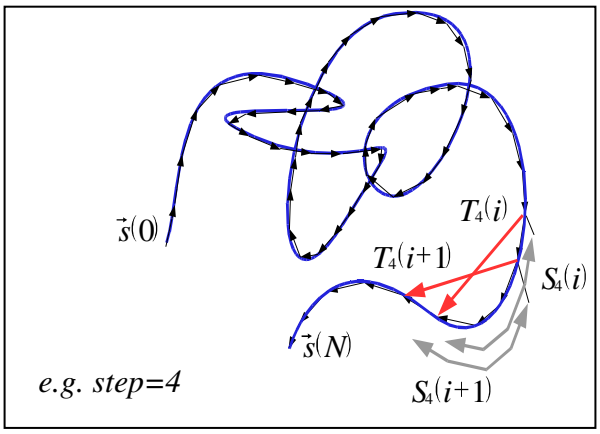

References

Debeir, O., Van Ham, P., Kiss, R., and Decaestecker, C. (2005). Tracking of migrating cells under phase-contrast video microscopy with combined mean-shift processes. IEEE Trans Med Imaging *24*, 697-711.

Debeir, O., Adanja, I., Kiss, R., and Decaestecker, C. (2008). Models of cancer cell migration and cellular imaging and analysis. In C. Ampe & A. Lambrechts (eds), "The motile actin system in health and disease", Transworld Research Signpost: Kerala, India, pp. 123-156.

Jang, D.H., Han, J.H., Lee, S.H., Lee, Y.S., Park, H., Kim, H., and Kaang, B.K. (2005). Cofilin expression induces cofilin-actin rod formation and disrupts synaptic structure and function in Aplysia synapses. Proc Natl Acad Sci U S A *102*, 16072-16077.

Sidani, M., Wessels, D., Mouneimne, G., Ghosh, M., Goswami, S., Sarmiento, C., Wang, W., Kuhl, S., El-Sibai, M., Backer, J.M., Eddy, R., Soll, D., and Condeelis, J. (2007). Cofilin determines the migration behavior and turning frequency of metastatic cancer cells. J Cell Biol *179*, 777-791.